Heliyon 8 (2022) e11383

Contents lists available at ScienceDirect

Heliyon

journal homepage: www.cell.com/heliyon

Research article

Differentiating malignant pleural mesothelioma and metastatic pleural disease based on a machine learning model with primary CT signs: A multicentre study

Ye Li [a,1], Botao Cai [b,1], Bing Wang [c], Yan Lv [a], Wei He [a], Xiaoxia Xie [b], Dailun Hou [a,*]

[a] Department of Radiology, Beijing Chest Hospital, Capital Medical University, Beijing, 101149, China
[b] Department of Radiology, Harbin Chest Hospital, Harbin 150000, China
[c] Department of Radiology, Beijing Tuberculosis and Thoracic Tumor Research Institute, Beijing, 101149, China

ARTICLE INFO

Keywords:
Malignant pleural mesothelioma
Metastatic pleural disease
Computer tomography
Machine learning

ABSTRACT

Rationale and Objectives: It is still a challenge to make confirming diagnosis of malignant pleural mesothelioma (MPM), especially differentiating from metastatic pleural disease (MPD). The aim of this study was to develop a model to distinguish MPM with MPD based on primary CT signs.

Materials and methods: We retrospectively recruited 150 MPM patients and 147 MPD patients from two centers and assigned them to training (115 MPM patients and 113 MPD patients) and testing (35 MPM patients and 34 MPD patients) cohorts. The images were analyzed for pleural thickening, hydrothorax, lymphadenopathy, thoracic volume and calcified pleural plaque (CPP). The selected clinical characteristics and primary CT signs comprised the model by multivariate logistic regression in the training cohort. Then the model was tested on the external testing cohort. ROC curve and F1 score were used to validate the capability of the model in both two cohorts.

Results: There were significant differences between two groups: (1) carcinoembryonic antigen (CEA); (2) nodular and mass pleural thickening; (3) the enhancement of pleura; (4) focal, diffuse and circumferential pleural thickening; (5) the thickest pleura; (6) thickening of diaphragmatic pleura; (7) multiple nodules and effusion of interlobar pleura; (8) hilar LN and ring enhancement of LN; (9) punctate and stipe CPP. The AUC and F1 score of the model were 0.970 and 0.857 in the training cohort, 0.955 and 0.818 in the testing cohort.

Conclusion: The model holds promise for use as a diagnostic tool to distinguish MPM from MPD.

1. Introduction

Malignant pleural mesothelioma (MPM) is an infrequent and aggressive thoracic malignancy with poor prognosis that originated from the lining of the chest cavity [1]. MPM is not only the most common primary pleural neoplasm but also accounting for 70%–90% of all malignant mesotheliomas [1]. Besides, the median overall survival of patients with advanced surgically unresectable disease is approximately 12-months [2]. The best outcome was possible with early detection, accurate staging and therapy response assessment [3].

Metastatic pleural disease (MPD) is a type of cancer spread from another organ to the pleura surrounding the lungs like lung and breast [3]. It can be challenging to differentiate MPM from MPD either on clinical or on imaging. Histologic sampling by needle aspiration pleural biopsy tests or thoracoscopic surgery was necessary for diagnosing MPM [4]. However, the pathological diagnosis of MPM may be difficult and immune-histological or ultra-structural analysis is required to differentiate MPM from MPD [5]. Chest radiography and computed tomography (CT) imaging are used to examine patients with pleural diseases and the most common method for show great importance especially in uncertain pathologic diagnosis or incapable of receiving biopsy [6]. CT has shown good performance as a diagnostic tool and staging of MPM. Although CT is the first-line imaging modality for the evaluation of MPM, many benign and malignant pleural diseases such as MPD, tuberculous pleurisy and empyema may cause pleural abnormalities that resemble MPM [7]. As a result, it is often difficult to make confirming diagnosis. Several previous studies have compared MPM with MPD [6, 7]. There have been different viewpoints in meaningful CT findings and significant overlap between

* Corresponding author.
E-mail address: hou.dl@mail.ccmu.edu.cn (D. Hou).
[1] These authors contributed equally to this work.

https://doi.org/10.1016/j.heliyon.2022.e11383
Received 19 July 2022; Received in revised form 9 October 2022; Accepted 28 October 2022

the two persists especially in the type and scope of pleural thickening, hydrothorax and lymphadenopathy.

The CT signs of MPM and MPD may be useful for discriminating these two diseases. As a result, the aim of this study was to evaluate whether CT signs could differentiate MPM from MPD and develop a machine learning model based on primary CT signs and clinical characteristics.

2. Materials and methods

2.1. Participants

The ethics committee of Beijing Chest Hospital, Capital Medical University approved all the data in the study for retrospective analysis and waived the demand for informed consent.

In the study, all patients which were enrolled met the inclusion criteria: (a) pathologic confirmation based on pleural tissue samples obtained by thoracoscopic pleural biopsy, open thoracotomy or sonography or CT-guided needle biopsy of the pleura. (b) All patients underwent enhanced chest CT with informed consent; (c) all CT scans were performed before biopsy, chemotherapy, radiotherapy or surgery. The exclusion criteria included the following: (a) poor image quality or motion artefact; (b) no visible pleural lesions on CT images; (c) incomplete CT images or clinical information.

Finally, a total of 150 patients with MPM and 147 patients with MPD. More specifically, 115 patients with MPM and 113 patients with MPD were comprised the training cohort from May 2013 to December 2018 in Beijing Chest Hospital, Capital Medical University. All MPD patients had lung cancer (101 adenocarcinomas, 5 squamous cell carcinomas and 7 small cell lung cancers). In addition, a independent testing cohort which included 35 patients with MPM and 34 patients with MPD from January 2019 to January 2022 in Harbin Chest Hospital was subsequently enrolled. The 34 MPD patients in the testing cohort had lung cancer (31 adenocarcinomas, 1 squamous cell carcinoma and 2 small cell lung cancers). The flowchart of patient recruitment was displayed in Figure 1.

2.2. CT image acquisition

All CT scans were performed with an Optima CT 680 system or Revolution CT (GE Healthcare, Milwaukee, WI, USA). Scanning was performed from the tip of the lung to the posterior costophrenic angle. The scanning parameters which were included 120 kV tube voltage, automatic tube current modulation, 64 × 0.625 mm detector collimation, 500 ms rotation time and 1.375 spiral pitch factor. The image reconstruction parameters which were included 1.25 mm slice thickness, 1.25 mm increment, 15 cm field of view, and 512 × 512 matrix. Simultaneously, all patients underwent contrast-enhanced CT scanning. 80 mL of nonionic contrast material (Iopamidol, 300 mgI/mL) was injected intravenously at a flow rate of 2.5–3.0 mL/s. The images were obtained from the enhanced scan, which were performed after the injection of 80 ml contrast agent.

2.3. Image analysis

All images were analyzed on AW 4.7 workspace station. Original transverse and post-processed images which included maximum intensity projection (MIP) and multiple-planar reconstruction (MPR) images of each patient were independently reviewed by two radiologists with at least 10 years of experience in analyzing chest images who were blinded to the final diagnosis. The primary signs were as follows:

(a) Pleural thickening included thin smooth thickening (thickest point with a short diameter between 3 and 10 mm), nodular (irregular thickening focally with a short diameter between 10 and 30 mm), mass (focal pleura-based lesion with a short diameter of >30 mm) [8]. Besides, we analyzed the scope of pleural thickening, which was classified as thickening focally (thicken with less than one lobe) and diffuse thickening (continuous pleural thickening involved more than one lobe). As for diffuse thickening, we independently evaluated circumferential thickening which was

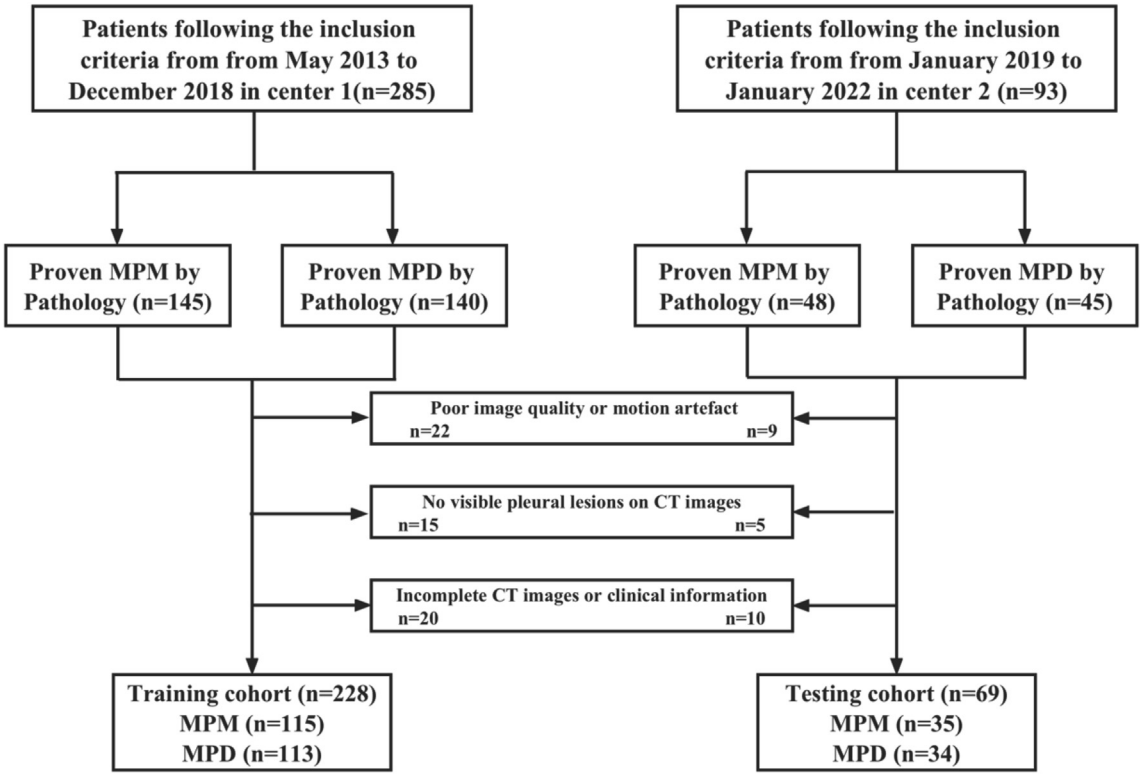

Figure 1. Flowchart of patient selection.

defined as continuous pleural thickening surrounded more than three-quarters of the hemithorax, including an intercostal and mediastinal pleura. The thickening and effusion of pleura mediastinalis and interlobar pleural were independently recorded according to the above criteria.

(b) The volume and density of hydrothorax were documented. It was considered hyperdense when more than 20 HU and hypo when less. The volume of hydrothorax was classified as mild, moderate and large, which was separately defined as filling less than one-third, between one-third and two-thirds and more than two-thirds of the hemithorax.

(c) The enlargement and enhancement of lymph nodes (LN) were also documented. The lymphadenopathy was defined as the short axis diameter was more than 1 cm in the mediastinal, hilar and abdominal LN. Cardiophrenic LN was considered enlarged if greater than 5 mm in short axis. Internal mammary LN was considered abnormal if larger than the accompanying vessels, and retropleural LN was considered abnormal if detected. In addition, the presence of calcification, necrosis and ring enhancement of LN was also looked for.

(d) The decrease of thoracic volume and mediastinal shifting were separately evaluated. The decrease of thoracic volume was defined as decreased volume of hemithorax in the involved side compared with opposite side. Mediastinal shifting was defined as the dislocation of mediastinal structures due to pleural lesions.

(e) Pleural plaque was defined as variable-size localized calcific densities or pleural thickening of soft tissue less than 5 cm in length attached along the pleura of the chest wall [9]. We recorded calcified pleural plaque (CPP) in the involved side of pleural disease. Besides, CPP was classified as punctate, stripe and patchy [10].

2.4. Statistical analysis and model construction

SPSS software (version 25) and the Python Scikit-learn package were used to analyze the data. We used kappa test to evaluate the two radiologists agreements of primary CT signs (k values of poor, fair, moderate, substantial, and near-perfect agreement were <0.00, 0.21–0.40, 0.41–0.60, 0.61–0.80, and 0.81–1.00, respectively). Difference of basic clinical characteristics and primary CT signs was assessed using Mann-Whitney U tests or t tests for continuous variables and the Pearson chi-square tests for categorical variables. Statistical tests were conducted with $p < 0.05$ as an indicator of statistical significance. Logistic regression was a traditional machine learning model commonly employed in medical applications to interpret clinical data in depth and recently used in the field. The selected features were used to build a model by multivariate logistic regression in the training cohort, which included the optimum CT signs and clinical variables with significant differences. The training cohort was randomly divided into two parts by the ratio of 7:3 using tenfold cross validation to train and validate the model. Finally, we selected the best model and tested it on the external testing cohort. The performance of the model in both cohorts was evaluated with receiver operator characteristic (ROC) curves, and the area under the curve (AUC) was calculated. In addition, the accuracy, precision (positive predictive value), recall (sensitivity) and F1 score were calculated and documented in both cohorts.

3. Results

3.1. Patient clinical characteristics

There was significant difference in CEA between MPM patients and MPD patients in both the training cohort and testing cohort ($p < 0.05$). As shown in Table 1, the remaining clinical characteristics, including age, gender, family medical history and smoking history had no significant difference in either the training cohort or the testing cohort.

3.2. Primary CT signs (Table 2)

There was excellent interobserver agreement with regard to the primary signs of pleural thickening, pleural effusion, LN, thoracic volume, mediastinal shifting and pleural plaque which k values were 0.845, 0.791, 0.763, 0.812, 0.897 and 0.868, respectively.

3.3. Pleural thickening

Most MPM and MPD patients had pleural thickening. Specifically, there were significant differences in nodular (Figure 2a) and mass thickening (Figure 2e) between two groups ($p < 0.05$) in the training cohort, nodular thickening had not been significant difference in the testing cohort. As for the scope of pleural thickening, diffuse (Figure 2d) and circumferential thickening (Figure 2c) were more frequently observed in MPM patients than MPD patients in both two cohorts ($p < 0.05$). On the contrary, thickening focally (Figure 2b) was more common in MPD patients ($p < 0.05$). Besides, the pattern of enhancement had significant differences between two groups. The homogeneous enhancement of pleura was more common in MPM ($p < 0.05$) and the heterogeneous enhancement of pleura was more frequently observed in MPD ($p < 0.05$).

There were significant differences in thickening of diaphragmatic pleura (Figure 2f) and interlobar pleura (Figure 3a), multiple nodules of interlobar pleura (Figure 3b) and interlobar pleural effusion (Figure 3c) ($p < 0.05$). However, multiple nodules of interlobar pleura and interlobar pleural effusion had not been significant differences in the testing cohort.

3.4. Hydrothorax

The density and volume of hydrothorax had no significant differences between two groups in both two cohorts.

3.5. Lymphadenopathy

Among the lymphadenopathy, there were significant differences in hilar LN (Figure 4a) and the ring enhancement of LN in the training cohort. The remaining signs including the ring enhancement of LN in the testing cohort had no significant differences between two groups.

3.6. CPP

The punctate (Figure 4b) and stripe (Figure 4c) CPP had significant differences between two groups in the training cohort. In the testing cohort, stipe CPP had not been significant difference. There was no significant difference in patchy CPP between two groups in two cohorts.

3.7. Model performance

Finally, the significant clinical characteristics and primary CT signs were comprised to build the model. As shown in Figure 5, the model showed a favourable performance for discriminating two diseases in the training cohort, with AUCs and F1 scores of 0.970 and 0.857, 0.955 and 0.818 in the training and testing cohort respectively. Besides, we calculated the accuracy, precision and recall of the model, which was separately 0.842, 0.900 and 0.818 in the training cohort and 0.826, 0.818 and 0.818 in the testing cohort.

4. Discussion

In the present study, we evaluated primary CT signs of pathologically confirmed MPM and MPD. The analysis of CT signs was more detailed than previous study [6]. Then significant primary CT signs and clinical characteristics were selected to build a machine learning model for differentiating MPM from MPD, which showed a good discriminate ability in an independent external testing cohort.

Table 1. Clinical characteristics of MPM and MPD patients in training and testing cohort.

Clinical characteristics	Training cohort		p-value	Testing cohort		p-value
	MPM (n = 115)	MPD (n = 113)		MPM (n = 35)	MPD (n = 34)	
Gender						
Male	73 (63.48)	70 (61.95)	0.811	22 (62.86)	21 (61.76)	0.925
Female	42 (36.52)	43 (38.05)		13 (37.14)	13 (38.24)	
Age (mean ± SD years)	62.50 ± 11.28	60.02 ± 11.06	0.230	62.42 ± 13.88	57.82 ± 12.07	0.408
Family medical history	6 (5.22)	11 (9.73)	0.194	2 (5.71)	3 (8.82)	0.618
Smoking history	54 (46.96)	41 (36.28)	0.102	16 (45.71)	12 (35.29)	0.378
CEA M (Q1, Q3) nmol/L	1.61 (1.10, 2.21)	7.64 (2.64, 40.71)	0.000*	1.79 (0.87, 2.32)	7.69 (3.46, 14.98)	0.000*

Note: Differences were assessed by t test, Mann-Whitney U test or chi-square test. SD: standard deviation. *p < 0.05.

Table 2. Primary CT signs from MPM and MPD patients in training cohort and testing cohort.

CT signs	Training cohort		p-value	Testing cohort		p-value
	MPM (n = 115)	MPD (n = 113)		MPM (n = 35)	MPD (n = 34)	
Pleural thickening						
Thin smooth	21 (18.26)	23 (20.35)	0.689	6 (17.14)	7 (20.59)	0.714
Nodular	69 (60.00)	88 (77.88)	0.004*	19 (54.29)	26 (76.47)	0.053
Mass	23 (20.00)	2 (1.77)	0.000*	8 (22.86)	0 (0.00)	0003*
Homogeneous enhancement	36 (31.30)	14 (12.39)	0.001*	11 (31.43)	4 (12.90)	0.048*
Heterogeneous enhancement	42 (36.52)	88 (77.88)	0.000*	13 (37.14)	25 (73.53)	0.002*
The scope of pleural thickening						
Thickening focally	27 (23.48)	68 (60.18)	0.000*	8 (22.86)	20 (58.82)	0.002*
Diffuse	86 (74.78)	45 (39.82)	0.000*	26 (74.29)	14 (41.18)	0.005*
Circumferential	54 (46.96)	16 (14.16)	0.000*	16 (45.71)	5 (14.71)	0.005*
The thickest pleura (mean ± SD mm)	17.27 ± 13.55	10.26 ± 5.93	0.000*	17.08 ± 15.76	6.18 ± 4.09	0.035*
Thickening of diaphragmatic pleura	75 (65.22)	43 (38.05)	0.000*	23 (65.71)	13 (38.24)	0.022*
Thickening of interlobar pleura	101 (87.8)	90 (79.65)	0.094	31 (88.57)	27 (79.41)	0.299
Single nodule of interlobar pleura	4 (3.48)	2 (1.77)	0.420	1 (2.86)	0 (0.00)	0.321
Multiple nodules of interlobar pleura	59 (51.30)	83 (73.45)	0.001*	18 (51.43)	25 (73.53)	0.058
Interlobar pleural effusion	35 (30.43)	14 (12.39)	0.001*	10 (28.57)	4 (12.90)	0.083
Hydrothorax						
High-density	3 (2.61)	1 (0.88)	0.322	0 (0.00)	0 (0.00)	
Low-density	103 (89.6)	105 (92.9)	0.371	31 (88.57)	30 (88.24)	0.720
Mild	90 (78.26)	92 (81.42)	0.553	27 (77.14)	28 (82.35)	0.591
Moderate	10 (8.70)	6 (5.31)	0.317	3 (8.57)	2 (5.88)	0.667
Large	6 (5.22)	8 (7.10)	0.558	1 (2.86)	1 (2.94)	0.983
Lymphadenopathy						
Mediastinal	58 (50.43)	66 (58.41)	0.227	19 (54.29)	20 (58.82)	0.704
Hilar	13 (11.30)	45 (39.82)	0.000*	4 (11.43)	13 (38.24)	0.010*
Abdominal	2 (1.74)	6 (5.31)	0.143	0 (0.00)	2 (5.88)	0.145
Cardiophrenic	12 (10.43)	10 (8.85)	0.685	3 (8.57)	3 (8.82)	0.970
Internal mammary	8 (6.96)	4 (3.54)	0.248	4 (11.43)	2 (5.88)	0.414
Supraclavicular	12 (10.43)	10 (8.85)	0.685	4 (11.43)	3 (8.82)	0.720
LN with necrosis	13 (11.30)	10 (8.85)	0.538	3 (8.57)	2 (5.88)	0.667
Calcified LN	15 (13.04)	8 (7.10)	0.135	4 (11.43)	1 (2.94)	0.174
Ring enhancement of LN	1 (0.87)	8 (7.10)	0.016*	0 (0.00)	2 (5.88)	0.145
Decrease of thoracic volume	19 (16.52)	17 (15.04)	0.760	6 (17.14)	5 (14.71)	0.782
Mediastinal shifting	17 (14.78)	25 (22.12)	0.153	5 (14.29)	7 (20.59)	0.490
CPP						
Punctate	25 (21.74)	2 (1.77)	0.000*	8 (22.86)	0 (0.00)	0.003*
Stripe	21 (18.26)	4 (3.54)	0.000*	6 (17.14)	1 (2.94)	0.051
Patchy	4 (3.48)	1 (0.88)	0.181	1 (2.86)	0 (0.00)	0.321

Note: Differences were assessed by chi-square test. *p < 0.05. SD: standard deviation.

We analyzed basic clinical characteristics and discovered that the CEA of MPM patients had significant differences with MPD patients, whereas the other clinical characteristics including age, gender, family medical history and smoking history did not show a significant difference, similar to the results of previous studies [6]. The CEA expression of MPM patients seems to be down-regulated when compared with MPD patients. Besides, it seems that CEA is a negative predictor for MPM [11]. However, a low level of CEA alone can neither prove nor

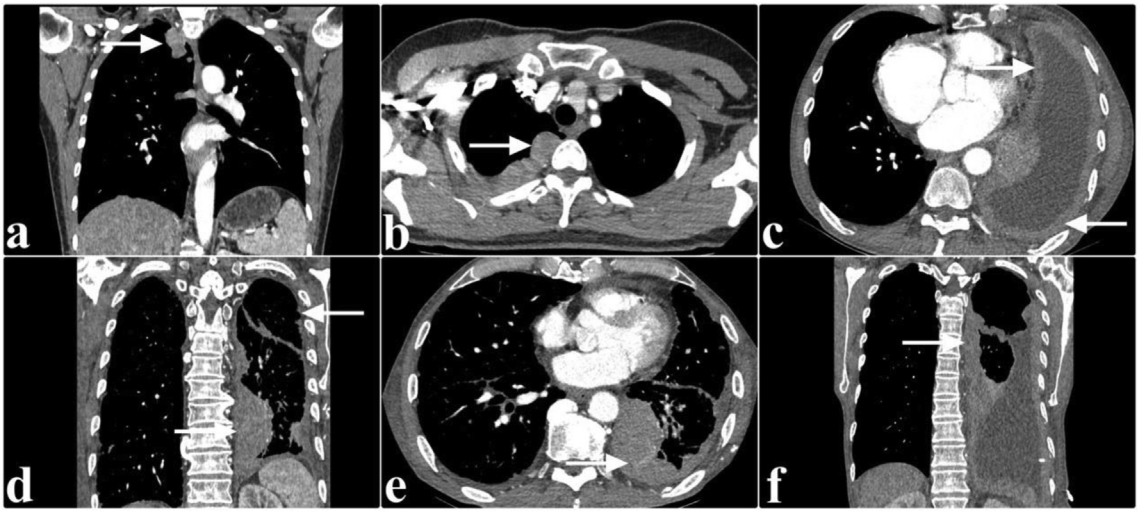

Figure 2. Axial and coronal CT section through the chest in a 44-year-old woman with MPD (a, b), 76-year-old man with MPM (d, e) and 77-year-old man with MPD (c, f). (a) Nodular pleural thickening (arrow), (b) pleural thickening focally, (c) Circumferential pleural thickening, (d) Diffuse pleural thickening, (e) mass pleural thickening and (f) Thickening of diaphragmatic pleura.

Figure 3. Axial through the chest in lung window in a 70-year-old man with MPM (a) and 40-year-old woman with MPM (b, c). (a) Thickening of interlobar pleura, (b) Multiple nodules of interlobar pleura, and (c) Interlobar pleural effusion.

Figure 4. Axial CT section through the chest in a 51-year-old woman with MPD (a), 65-year-old man with MPM (b) and 73-year-old man with MPM (c). (a) Enlarged hilar LN, (b) patchy CPP and (c) stripe CPP.

exclude MPM. On the contrary, MPD patients always have increased CEA serum levels [12].

The most common CT signs of MPM and MPD patients in our study was pleural thickening which was seen in approximately all patients except two MPM patients. These findings were greater prevalence in the current study which may be due to larger and different patient populations or the greater sensitivity with the use of thinner sections on multidetector CT scanners. Our study found that circumferential and diffuse pleural thickening was more frequent in MPM patients than MPD patients ($p < 0.05$) as well as several studies [6, 9]. It is reported that these two signs, especially circumferential pleural thickening was the most specific thickening for distinguishing MPM from MPD [10]. Mass pleural thickening was commonly seen in MPM patients and this was similar to previous studies [13, 14]. Nodular pleural thickening and multiple nodules of the interlobar pleura were thought to be more frequent in MPM patients. However, MPD patients were more commonly observed this sign in the training cohort and there was no significant difference in the testing cohort. Thickening of diaphragmatic pleura had significant differences between two groups. Our results are consistent with other studies [6]. It was valuable for differentiating MPM from MPD and the prevalence of it varied from 6.1 to 76% in MPM [15]. However, variation in prevalence may be caused by CT image quality and the availability of coronal reformatted images [16]. As for the enhancement of the pleura, MPM patients showed more homogeneous whether MPD patients showed more heterogeneous. This mainly caused by the rare necrosis and cystic degeneration in MPM patients [17].

Most patients had hydrothorax in our study. Both the density and amount of hydrothorax had no significant differences in two groups. Actually, the most frequent manifestation of metastatic pleural involvement was hydrothorax [18]. Besides, this was the second most common finding of two groups in either training cohort or testing cohort.

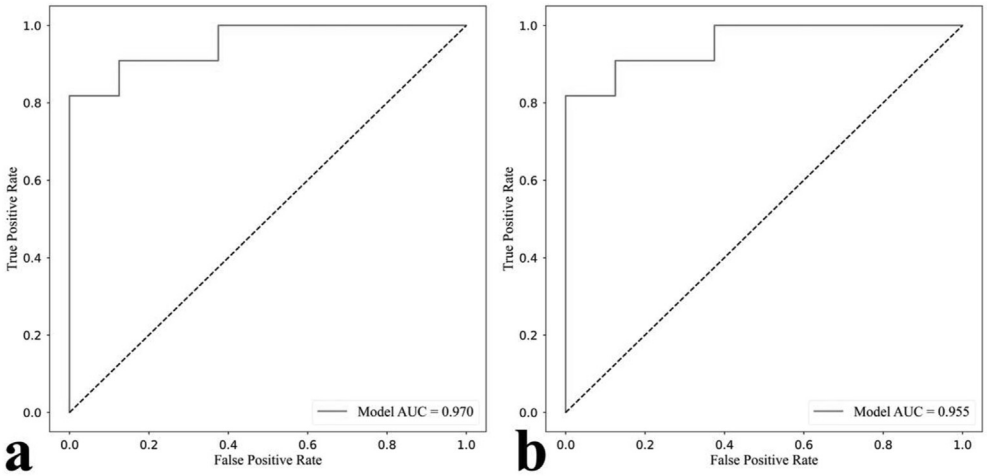

Figure 5. ROC curves of the model. (a) Training cohort (b) Testing cohort.

Hilar LN enlargement was more frequently observed in MPD patients as well as the previous study, which may have been related to the larger proportion of MPD patients with lung cancer [19]. The involvement of hilar LN always occurred secondary to parenchymal infiltration and drained lungs and visceral pleura which was not due to direct spread from pleura [20]. However, there were no significant differences in mediastinal, cardiophrenic, internal mammary, supraclavicular and abdominal LN between two groups. They were commonly drained parietal pleura and primarily involved in MPM. The prevalence of these LNs was similar to several studies [19, 20]. It is reported that the extrapleural LN especially with involvement of mediastinal pleura and decrease of thoracic volume had an important diagnostic value in early diagnosis of MPM [21]. In contrast, there were no significant difference in decrease of thoracic volume and mediastinal shifting between two groups in our current study.

CPP is the most common radiological manifestations of asbestos exposure [22]. However, the direct history of asbestos exposure was hidden. In our current study, only several patients were found to have a history of asbestos exposure. Then we found that the prevalence of indirect exposure to asbestos substances at work increased, which could lead to MPM. In some studies, CPP was defined as transverse or craniocaudal pleural thickening of <5 cm in length, whereas the definition of CPP used in the present study was based on review of the thin section, and coronal reformatted images [23]. We only evaluated CPP and the prevalence of CPP in MPM patients was similar to previous study. Besides, only 8 MPD patients in two cohorts had CPP. There were significant differences in CPP between two groups, especially punctate and stripe CPP.

There were many significant primary CT signs in current study, especially circumferential pleural thickening, mass pleural thickening, mediastinal pleural involvement and CPP, which were considered strongly suggestive of malignant pleural disease, but none are pathognomonic for MPM. As a result, we combined these significant CT signs with clinical characteristics to established a model. The model showed excellent classification power, whether in the training cohort or the testing cohort, whereas it was precise enough for clinical use. Besides, F1 score is also a great indicator for the classification of interest [24]. The model also showed an excellent performance whether in the training or testing cohort according to the F1 score. It indicates that the model was stable and general in routine clinical practice. This implies that the model will show good stability and generalizability in clinical practice.

However, there were several limitations in this study. First, this study was retrospective with a not large number of patients. Second, no enough pathological proof of LN metastasis, because although some patients underwent surgery, radiologic pathologic correlations were impossible for individual LN. Third, the created model of this current study only focus on primary CT signs, future study should focus on the quantitative analysis.

Differentiating MPM from MPD has been challenging thus far on CT with many overlapping findings. In conclusion, we created a model based on the clinical characteristics and primary CT signs which has significant value in differentiating MPM from MPD. Our model is potential, noninvasive, and effective complements to differentiate MPM from MPD based on clinical characteristics and primary CT signs.

Declarations

Author contribution statement

Ye Li: Conceived and designed the experiments; Analyzed and interpreted the data; Wrote the paper.

Botao Cai: Performed the experiments; Analyzed and interpreted the data.

Bing Wang; Yan Lv: Performed the experiments; Contributed reagents, materials, analysis tools or data.

Wei He; Xiaoxia Xie: Analyzed and interpreted the data; Contributed reagents, materials, analysis tools or data.

Dailun Hou: Conceived and designed the experiments; Contributed reagents, materials, analysis tools or data.

Funding statement

This research was supported by Leading Talents of Beijing Tongzhou District High Level Talent Development Support Project [YHLD2019029], Subproject of National Health Commission major project: tumor basis - lung cancer gene [2021-6].

Data availability statement

Data will be made available on request.

Declaration of interest's statement

The authors declare no conflict of interest.

Additional information

No additional information is available for this paper.

References

[1] J.L. Beebe-Dimmer, J.P. Fryzek, C.L. Yee, et al., Mesothelioma in the United States: a Surveillance, Epidemiology, and End Results (SEER)-Medicare investigation of treatment patterns and overall survival, Clin. Epidemiol. 8 (2016) 743–750.

[2] N.J. Vogelzang, J.J. Rusthoven, J. Symanowski, et al., Phase III study of pemetrexed in combination with cisplatin versus cisplatin alone in patients with malignant pleural mesothelioma, J. Clin. Oncol. 21 (14) (2003) 2636–2644.

[3] S. Cheng, T.L. Mohammed, Metastatic disease to the lungs and pleura: an overview, Semin. Roentgenol. 48 (4) (2013) 335–343.

[4] S. Cao, S. Jin, J. Cao, et al., Advances in malignant peritoneal mesothelioma, Int. J. Colorectal Dis. 30 (1) (2015) 1–10.

[5] S. Monaco, M. Mehrad, S. Dacic, Recent advances in the diagnosis of malignant mesothelioma: focus on approach in challenging cases and in limited tissue and cytologic samples, Adv. Anat. Pathol. 25 (1) (2018) 24–30.

[6] Y.K. Kim, J.S. Kim, K.W. Lee, C.A. Yi, J.M. Goo, S.H. Jung, Multidetector CT findings and differential diagnoses of malignant pleural mesothelioma and metastatic pleural diseases in Korea, Korean J. Radiol. 17 (4) (2016) 545–553.

[7] M. Metintas, I. Ucgun, O. Elbek, et al., Computed tomography features in malignant pleural mesothelioma and other commonly seen pleural diseases, Eur. J. Radiol. 41 (1) (2002) 1–9.

[8] J.M. Seely, E.T. Nguyen, A.M. Churg, N.L. Müller, Malignant pleural mesothelioma: computed tomography and correlation with histology, Eur. J. Radiol. 70 (3) (2009) 485–491.

[9] O. Tamer Dogan, I. Salk, F. Tas, et al., Thoracic computed tomography findings in malignant mesothelioma, Iran. J. Radiol. 9 (4) (2012) 209–211.

[10] Y. Kim, J.P. Myong, J.K. Lee, J.S. Kim, Y.K. Kim, S.H. Jung, CT characteristics of pleural plaques related to occupational or environmental asbestos exposure from south Korean asbestos mines, Korean J. Radiol. 16 (5) (2015) 1142–1152.

[11] T. Otoshi, Y. Kataoka, S. Ikegaki, et al., Pleural effusion biomarkers and computed tomography findings in diagnosing malignant pleural mesothelioma: a retrospective study in a single center, PLoS One 12 (10) (2017), e0185850.

[12] T. Muley, H. Dienemann, F.J. Herth, M. Thomas, M. Meister, J. Schneider, Combination of mesothelin and CEA significantly improves the differentiation between malignant pleural mesothelioma, benign asbestos disease, and lung cancer, J. Thorac. Oncol. 8 (7) (2013) 947–951.

[13] Z.J. Wang, G.P. Reddy, M.B. Gotway, et al., Malignant pleural mesothelioma: evaluation with CT, MR imaging, and PET, Radiographics 24 (1) (2004) 105–119.

[14] R.R. Gill, Imaging of mesothelioma, Recent Results Cancer Res. 189 (2011) 27–43.

[15] D. Halpenny, M. Raj, A. Rimner, J. Zheng, M. Capanu, M.S. Ginsberg, Computed tomography features of local pleural recurrence in patients with malignant pleural mesothelioma treated with intensity-modulated pleural radiation therapy, Eur. Radiol. 29 (7) (2019) 3696–3704.

[16] W.J. Yin, G.Q. Zheng, Y.F. Chen, et al., CT differentiation of malignant peritoneal mesothelioma and tuberculous peritonitis, Radiol. Med. 121 (4) (2016) 253–260.

[17] O. Lauk, M. Patella, T. Neuer, et al., Implementing CT tumor volume and CT pleural thickness into future staging systems for malignant pleural mesothelioma, Cancer Imag. 21 (1) (2021) 48.

[18] B. Feragalli, C. Mantini, N. Civitareale, R. Polverosi, A. Tartaro, A.R. Cotroneo, Extrapleural and cardiophrenic lymph nodes: prevalence, clinical significance and diagnostic value, Radiol. Med. 119 (1) (2014) 20–26.

[19] A.R. Abdel Rahman, R.M. Gaafar, H.A. Baki, et al., Prevalence and pattern of lymph node metastasis in malignant pleural mesothelioma, Ann. Thorac. Surg. 86 (2) (2008) 391–395.

[20] R. Gopar-Nieto, G. Aguilar-Madrid, L. Sotelo-Martínez, et al., Malignant pleural mesothelioma: accuracy of CT against immunohistochemical test among the Mexican population, Arch. Med. Res. 46 (2) (2015) 107–111.

[21] C.D. Strange, G.S. Shroff, J. Ahuja, I. Vlahos, M.F.K. Benveniste, M.T. Truong, Imaging of malignant pleural mesothelioma: Pearls and Pitfalls, Semin. Ultrasound CT MR 42 (6) (2021) 542–551.

[22] G.S. Meirelles, J.I. Kavakama, D. Jasinowodolinski, et al., Pleural plaques in asbestos-exposed workers: reproducibility of a new high-resolution CT visual semiquantitative measurement method, J. Thorac. Imag. 21 (1) (2006) 8–13.

[23] A. Bianco, T. Valente, M.L. De Rimini, G. Sica, A. Fiorelli, Clinical diagnosis of malignant pleural mesothelioma, J. Thorac. Dis. 10 (Suppl 2) (2018) S253–S261.

[24] G.H. Lee, S.Y. Shin, Federated learning on clinical benchmark data: performance assessment, J. Med. Internet Res. 22 (10) (2020), e20891.